Deconfinement phase transition in one-flavor QCD

Constantia Alexandrou,[1] Artan Boriçi,[2] Alessandra Feo,[1] Philippe de Forcrand,[3] Andrea Galli,[4] Fred Jegerlehner,[5] and Tetsuya Takaishi[6]

[1]*Department of Natural Sciences, University of Cyprus, CY-1678 Nicosia, Cyprus*
[2]*Paul Scherrer Institute, CH-5232 Villigen PSI, Switzerland*
[3]*Swiss Center for Scientific Computing, ETH-Zentrum, CH-8092 Zürich, Switzerland*
[4]*ELCA Informatique, Hofwiesenstrasse 26, CH-8057 Zürich, Switzerland*
[5]*DESY-IfH Zeuthen, D-15738 Zeuthen, Germany*
[6]*Hiroshima University of Economics, Hiroshima, Japan 731-01*

(Received 24 November 1998; published 30 June 1999)

We present a study of the deconfinement phase transition of one-flavor QCD using the multiboson algorithm. The mass of the Wilson fermions relevant for this study is moderately large and the non-Hermitian multiboson method is a superior simulation algorithm. Finite-size scaling is studied on lattices of size $8^3 \times 4$, $12^3 \times 4$, and $16^3 \times 4$. The behaviors of the peak of the Polyakov loop susceptibility, the deconfinement ratio, and the distribution of the norm of the Polyakov loop are all characteristic of a first-order phase transition for heavy quarks. As the quark mass decreases, the first-order transition gets weaker and turns into a crossover. To investigate finite-size scaling on larger spatial lattices we use an effective action in the same universality class as QCD. This effective action is constructed by replacing the fermionic determinant with the Polyakov loop identified as the most relevant $Z(3)$-symmetry-breaking term. Higher-order effects are incorporated in an effective $Z(3)$-breaking field h, which couples to the Polyakov loop. Finite-size scaling determines the value of h where the first-order transition ends. Our analysis at the end point h_{ep} indicates that the effective model and thus QCD are consistent with the universality class of the three-dimensional Ising model. Matching the field strength at the end point h_{ep} to the κ values used in the dynamical quark simulations we estimate the end point κ_{ep} of the first-order phase transition. We find $\kappa_{ep} \sim 0.08$ which corresponds to a quark mass of about 1.4 GeV. [S0556-2821(99)05313-8]

PACS number(s): 12.38.Gc, 11.15.Ha, 12.38.Mh, 64.60.Fr

I. INTRODUCTION

Understanding the properties of quantum chromodynamics (QCD) under extreme conditions of high temperature and/or pressure is a challenging problem and was considered long ago. Polyakov [1] and Susskind [2] predicted that QCD will undergo a deconfinement phase transition from normal hadronic matter to a quark-gluon plasma when the temperature is increased. Such a phase transition is believed to have occurred, in the opposite direction, 1 μs after the big bang and its nature is therefore important in astrophysics. Theoretical information on the deconfinement phase transition has also become important as planned ultrarelativistic experiments will soon start at the BNL Relativistic Heavy Ion Collider (RHIC), and later on at the CERN Large Hadron Collider (LHC). In these experiments the temperature reached will be of the order of 600 MeV and, at this temperature, one is still dealing with a strongly interactive system. Thus lattice QCD provides the most suitable nonperturbative approach to study such phenomena using directly the QCD Lagrangian.

The zero-flavor sector of the theory (quenched) has been studied extensively and it is established that there is a first-order deconfinement phase transition [3] with the critical temperature determined in the continuum limit [4–8]. State-of-the-art lattice calculations are now being done including pair creation. For two flavors ($N_f=2$) there are simulations both with Wilson [9] and staggered fermions [9,10] whereas for a greater number of flavors the simulations are usually performed with the standard Wilson action [10,11]. On the other hand, one-flavor QCD has been largely ignored (early exceptions are given in Ref. [12]), perhaps because of algorithm difficulties, although it has interesting properties. In the usual analysis the continuum $N_f=1$ theory is expected to have no chiral phase transition [13] because of the anomalous breaking of the U(1) chiral symmetry. We note, however, the unexpected results of a study of one-flavor staggered fermions [14] which may imply a chiral phase transition. The purpose of this work is to fill this gap by investigating the deconfinement phase transition of one-flavor QCD.

A model that plays an important role in our understanding of the phase diagram in QCD is the three-state Potts model in three dimensions. It has a $Z(3)$ symmetry and the spontaneous breakdown of this symmetry is expected to drive the deconfinement phase transition like it does in quenched QCD. In the presence of an external field the $Z(3)$ symmetry is explicitly broken just like the fermionic determinant breaks $Z(3)$ symmetry in QCD. In fact it was shown by DeGrand and DeTar [15] that, at high temperature and heavy quark mass, QCD reduces to the three-state Potts model in an external field. From its phase diagram [15], shown schematically in Fig. 1, we observe that the first-order phase transition gets weaker as the strength of the external field h increases and ends at some critical value h_{ep} with a second-order transition. Beyond this point a crossover behavior is seen. Whereas Fig. 1 gives us a good starting point for the expected qualitative behavior for QCD with dynamical quarks, the quantitative question of the existence of such an

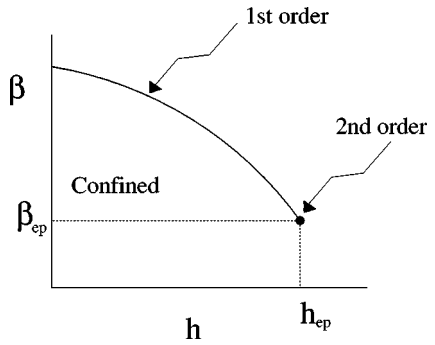

FIG. 1. Phase diagram in the three-state Potts model in three dimensions.

end point and its location can only be answered after a detailed calculation.

In the real world of two light quarks and one heavy quark the phase diagram depends crucially on the size of the light and heavy quark masses. Therefore it is usual to consider the phase diagram of three-flavor QCD in the mass plane m_s vs $m_{u,d}$. The mass point (0,0) is the chiral limit with a first-order transition. Pure gauge is the opposite limit of infinite quark masses where a first-order transition is also established. As one moves away from the infinite-mass (or hopping parameter $\kappa=0$) limit the first-order transition is expected, like in the Potts model, to persist but to become weaker and eventually to disappear, as the quark mass is reduced. This presumed robustness is based on the expectation that an infinitesimal increase in κ does not cause the finite gap in the thermodynamical observables to change discontinuously but smoothly. That a first-order transition is in general robust is supported from our experience with spin systems where a first-order transition remains first order for small magnetic fields. In this work we seek to determine the point on the line $(m_{u,d}=\infty, m_s)$ where the first-order transition ends as well as the universality class of the second-order phase transition at this end point. It turns out that the relevant quark masses for this study are relatively large and therefore the multiboson algorithm is a very efficient method for simulating such dynamical quarks.

From the determination of the end point for one flavor we can draw conclusions about the end point for two flavors, i.e., where on the line $(m_{u,d}, m_s=\infty)$ the first-order transition ends. The quark mass where this is expected to occur is about twice the mass obtained in the one-flavor case because the quark effects that we observe are about half as large as the effects obtained for two flavors of the same mass.

In order to determine quantitatively the phase diagram for QCD we perform simulations on lattices with size $8^3\times4$, $12^3\times4$, and $16^3\times4$. Performing a finite-size scaling analysis we find indeed that there is a first-order phase transition for heavy quarks which gets weaker as the quark mass decreases and becomes second order at a value of $\kappa_{ep}\sim0.08$. For smaller quark masses a crossover behavior is seen [16].

In order to determine the end point in the (β,κ) plane accurately one needs larger lattice sizes, which takes very long to simulate. However, there is a different route that we can follow. Namely, we investigate an effective model in the same universality class as QCD which is easier to simulate, determine the end point there, and then match back to QCD. Such an effective model can be constructed by taking the pure gauge action and adding the most relevant $Z(3)$-breaking term which is a Polyakov loop. The strength of the $Z(3)$-breaking field is adjusted to model higher-order terms. Within this effective model we were able to perform a finite-size scaling analysis up to a lattice size of 24^3 and determine the critical strength of the $Z(3)$-breaking field where the first-order transition ends. We also investigated the lattice spacing dependence within the effective model, by performing a simulation for temporal extension $N_t=2$ in addition to $N_t=4$. Finite-size scaling at the end point h_{ep} yields results that are consistent with the scaling behavior seen in the three-dimensional Ising model. We obtain $h(\kappa)$ by performing a best fit of the Polyakov loop histograms obtained in the effective model to those obtained in QCD. This nonperturbative matching of h_{ep} yields the critical value of κ_{ep} and of β_{ep}.

This paper is organized as follows: In Sec. II we give details of the local bosonic algorithm which we used to simulate one dynamical Wilson fermion. In Sec. III we describe the observables that we used to probe a change of phase and the nature of this phase transition. We give the results of this analysis in Sec. IV. In Sec. V we discuss the simulation and the finite-size scaling analysis of the effective model and connect it to full QCD. In Sec. VI we discuss the continuum limit and finally in Sec. VII we summarize and conclude.

II. LOCAL BOSONIC ALGORITHM FOR ONE FLAVOR

The local bosonic algorithm was originally proposed by Lüscher [17] as an alternative method to the widely used hybrid Monte Carlo (HMC) algorithm to simulate dynamical quarks. The basic idea is the replacement of the fermionic determinant by a functional integral over n bosonic fields having a local action. If $Q=\gamma_5 D/(1+8\kappa)$ where D is the fermionic Wilson matrix, then for two degenerate flavors we have

$$\det Q^2 \propto \lim_{n\to\infty} \int \prod_{k=1}^{n} d\phi_k^\dagger d\phi_k \times \exp\left(-\sum_{k=1}^{n} \phi_k^\dagger [(Q-\mu_k)^2+\nu_k^2]\phi_k \right), \quad (1)$$

where $\sqrt{z_k}=\mu_k+i\nu_k$ with z_k being the roots of a polynomial of even degree n constructed so that

$$\lim_{n\to\infty} P_n(Q^2)=\frac{1}{Q^2}. \quad (2)$$

The error introduced by taking n finite can be eliminated by a global accept-reject Metropolis test [18]. The generalization to any number of flavors is made possible by finding a polynomial approximation to the fermionic matrix itself rather than to Q^2 [18,19]. This can be done by constructing a

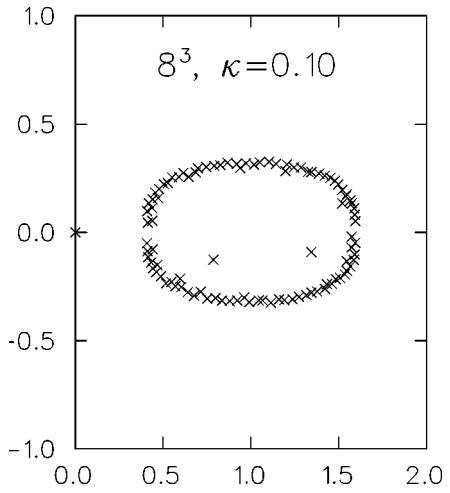

FIG. 2. Estimated boundary of the Dirac eigenvalue spectrum.

polynomial of even degree n defined in the complex plane with complex conjugate roots z_k such that

$$\lim_{n\to\infty} P_n(z)=\frac{1}{z} \tag{3}$$

for any z in the domain containing the spectrum of D (not including the origin). Since the spectral radius of the hopping matrix M is bounded by 8 in the free case and even less in the interacting case, we are guaranteed that the spectrum of $D=1-\kappa M$ will remain in the complex right half-plane for the heavy to moderately heavy quarks that we simulate ($\kappa \leqslant 1/8$). This is demonstrated in Fig. 2 where the boundary of the spectrum of the Dirac matrix is estimated for $\kappa=0.1$ as in Ref. [20].

Using the property $D=\gamma_5 D^\dagger \gamma_5$ we obtain

$$\det P_n(D)=c_n\prod_{k=1}^{n/2} \det(D-z_k)^\dagger \det(D-z_k), \tag{4}$$

with c_n an easily computed constant [19]. Instead of Eq. (1) one now finds

$$\det D=\lim_{n\to\infty}\det{}^{-1}[T_{n/2}^\dagger(D)T_{n/2}(D)]\propto \lim_{n\to\infty}\int\prod_{k=1}^{n/2} d\phi_k^\dagger d\phi_k \times\exp\left(-\sum_{k=1}^{n/2}\phi_k^\dagger(D-z_k)^\dagger(D-z_k)\phi_k\right), \tag{5}$$

where $T_{n/2}(D)=\Pi_{k=1}^{n/2}(D-z_k)$. The algorithm is made exact with a global Metropolis test as follows. The one-flavor determinant can be expressed as

$$\det D=\mathcal{C}\det{}^{-1}[T_{n/2}^\dagger(D)T_{n/2}(D)], \tag{6}$$

with the correction factor $\mathcal{C}$ given by

$$\mathcal{C}=\lim_{m\to\infty}\frac{\det{}^{-1}[T_{m/2}^\dagger(D)T_{m/2}(D)]}{\det{}^{-1}[T_{n/2}^\dagger(D)T_{n/2}(D)]}. \tag{7}$$

Because the error of the polynomial approximation (3) decreases exponentially with the degree of the polynomial, it is not necessary to actually take the limit $m\to\infty$ above. We observed that taking $m\geqslant 3n$, where n is adjusted for sufficient Metropolis acceptance below, is enough to make the systematic approximation error completely negligible compared to the statistical one. We implemented the correction factor $\mathcal{C}$ by a noisy Metropolis test, along the lines suggested in Ref. [18]. The gauge and boson fields (U,ϕ) are updated by a sequence of local Monte Carlo steps forming a trajectory $(U,\phi)\to(U',\phi')$. This procedure satisfies detailed balance with respect to the approximate action

$$S_{\text{approx}}=S_g[U]+\sum_{k=1}^{n/2}|(D-z_k)\phi_k|^2. \tag{8}$$

At the end of each trajectory, one generates a field η with probability

$$P^{HB}(\eta)=Re^{-|X\eta|^2}, \tag{9}$$

where $X=T_{m/2}(D)T_{n/2}^{-1}(D)$ and R is a normalization constant. The new configuration (U',ϕ') is accepted with probability

$$P^A_{(U,\phi)\to(U',\phi')}=\min\left[1,\frac{e^{-|X'\eta|^2}}{e^{-|X\eta|^2}}\right]. \tag{10}$$

The correction term is thus estimated by only one η field. Detailed balance with respect to the desired action $\det{}^{-1}[T_{m/2}^\dagger(D)T_{m/2}(D)]e^{-S_g[U]}$ is satisfied after averaging the probability density for the Metropolis test, $P^{HB}(\eta)P^A_{(U,\phi)\to(U',\phi')}$, over the η field.

The number of bosonic fields n is chosen so that the correction term leads to an acceptance rate of about 2/3 and m is taken at least 3 times n.

For the local updating of the gauge and boson fields we used standard heat bath and overrelaxation algorithms as described in [18]. A trajectory is a symmetric combination of $(2l+1)$ overrelaxation steps applied alternatively to the gauge and boson fields, preceded and followed by a heat bath on the bosons. Ergodicity for the gauge fields is maintained due to their coupling to the bosonic fields. The roots z_k are distributed on a circle centered at (1,0). We implemented even-odd preconditioning to lower the number of bosonic fields needed for a given accuracy. To efficiently equilibrate the system, we start from thermalized quenched gauge configurations and initialize the boson fields by generating a Gaussian random vector χ and setting

$$\phi_k\leftarrow c_n D\prod_{l\neq k}^{n}(D-z_k)\ \chi. \tag{11}$$

III. SIGNALS FOR THE PHASE TRANSITION OR LACK THEREOF

QCD with infinitely heavy quarks, i.e., quenched, undergoes a first-order deconfinement transition corresponding to

the spontaneous breaking of the $Z(3)$ Polyakov loop symmetry [21]. Based on the Polyakov loop, given by the product of gauge links in the temporal direction,

$$L(\mathbf{n})=\frac{1}{3}\mathrm{Tr}\prod_{n_0=1}^{N_t} U_0(\mathbf{n},n_0), \tag{12}$$

which transforms under $Z(3)$ as $L(\mathbf{n})\rightarrow zL(\mathbf{n})$, one can construct a standard set of observables and order parameters. In particular, $\langle L\rangle=0$ in the $Z(3)$-symmetric, confined phase, and nonzero in the spontaneously broken, deconfined phase.

As explained in the Introduction, one expects this phase transition to persist in the presence of sufficiently heavy dynamical quarks. However, these dynamical quarks explicitly break the quenched $Z(3)$ symmetry, favoring the real Z_3 branch and inducing a nonzero Polyakov loop $\langle L\rangle>0$ even in the confined phase. The Polyakov loop and associated observables can no longer serve as an order parameter. The phase transition will be identified as a discontinuity in these observables, from one nonzero value to another, in the thermodynamic limit.

Furthermore, as also explained in the Introduction, this first-order phase transition is expected to become weaker and eventually disappear, as the quark mass is reduced. The correlation length at criticality will correspondingly increase, and eventually diverge at the end point of the transition line where the transition becomes second order. For yet lighter quarks, no singularity appears even in the thermodynamic limit, and a simple crossover occurs in $\langle L\rangle$. The distinction between weak first-order, second-order, or crossover behavior requires lattice sizes at least comparable with the critical correlation length. However, this requirement can be lessened if one compares results for various small size lattices with a finite-size scaling ansatz. This is how the first-order nature of the quenched transition was first ascertained [3], and this is how we proceed here.

Our strategy is to vary β, for each quark mass, for three spatial lattice sizes and to look for the following signals.

Coexistence of the two phases. A distinctive feature of a first-order transition is phase coexistence and on a finite lattice we look for tunneling between the confined and deconfined phases which is observed over a small temperature range around the critical temperature. As the size of the lattice increases tunneling is exponentially suppressed but for the lattice sizes studied here enough tunneling events are observed to enable us to study the double-peak distribution for the norm $|\Omega|$ of the Polyakov loop defined as

$$\Omega=\frac{1}{V}\sum_{\mathbf{n}} L(\mathbf{n}), \tag{13}$$

with V the spatial volume. For a first-order phase transition, the location of the peaks should be fixed as the volume increases, while their width should decrease like V^{-1}. For a second-order phase transition or a crossover, the peaks should merge as the volume increases, and the tunneling signal should disappear.

Deconfinement ratio. The deconfinement ratio is defined by

$$\rho=\frac{3}{2}p-\frac{1}{2}, \tag{14}$$

with p the probability for the complex Polyakov loop to be within 20° of a Z_3 axis. Therefore, if the $Z(3)$ symmetry is unbroken, we find $p=1/3$ and $\rho=0$, whereas if it is broken in such a way that the Polyakov loop is distributed near one axis (the real axis), we have $p=1$ and $\rho=1$. The value of $\rho=0$ is only obtained in the quenched case where the $Z(3)$ symmetry is exact. With dynamical quarks we only look for a discontinuity across the phase transition. On a finite lattice, the discontinuity is smoothed out. $\langle\rho\rangle$ varies abruptly over a range in β which shrinks as V^{-1}, and the slope $d\rho/d\beta$ is maximum at the critical β. The intersection of curves $\rho(\beta)$ for various lattice sizes may also give information on β_c.[1]

The real part of the Polyakov loop after projection on the closest Z_3 axis. This observable is also an order parameter for the quenched phase transition. It behaves just like the deconfinement ratio in the presence of dynamical quarks.

The peak value of the susceptibility. The susceptibility measures the fluctuations of the Polyakov loop. We consider the behavior of

$$\chi_L=V(\langle|\Omega|^2\rangle-\langle|\Omega|\rangle^2), \tag{15}$$

which diverges at criticality for a first-order phase transition in the thermodynamic limit. On a finite lattice, instead of this δ function behavior, the peak value of χ_L is proportional to the volume V, while the width of the χ_L distribution scales like V^{-1} and its peak may shift like V^{-1} [22]. The scaling behavior of the susceptibility changes for a second-order transition: the peak value of χ_L becomes proportional to V^{α} with $\alpha<1$. For a crossover behavior where, even in the thermodynamic limit, there is no discontinuity in the thermodynamic functions, the peak value of χ_L remains constant with the volume.

IV. RESULTS

In Table I we collect the parameters of our simulations. Adjusting the number of bosonic fields, n, so that the acceptance is about 2/3, we can make two observations: First, for a fixed quark mass we find that n grows logarithmically with the volume for the same acceptance ratio (i.e., for the same relative error in the bosonic approximation of the determinant). This is illustrated in Fig. 3 which shows the $\kappa=0.1$ data from Table I. Second, for a fixed volume, n is approximately inversely proportional to the quark mass; i.e., $1/n$ is linear in $1/\kappa$. This behavior is displayed in Fig. 3 where it holds for a range of κ values. This dependence of n on both the quark mass and the volume confirms the expectations of, e.g., Ref. [23].

Our results for the observables which we used to decide on the order of the transition are shown in Figs. 4–7. In Fig. 4 tunneling between the confined and the deconfined phase is

[1]One complication here is that $\langle\rho\rangle$ in the confined phase depends on the spatial volume V.

TABLE I. In the first column we give the κ values for the three volumes studied. In the other columns n is the number of bosonic fields and acc the average acceptance; Ksw gives (in kilosweeps) the total number of thermalized configurations used in the reweighting procedure [24].

	$8^3\times4$		$12^3\times4$		$16^3\times4$	
κ	n/acc	Ksw	n/acc	Ksw	n/acc	Ksw
0.05	8/0.78	18	12/0.74	20	24/0.83	20
0.10	16/0.67	45	24/0.63	50	32/0.67	37
0.12	24/0.74	55	32/0.67	40	40/0.69	12
0.14	32/0.77	60	40/0.70	37	50/0.67	12

clearly observed for $\kappa=0.1$. A similar behavior is also found in the case of $\kappa=0.05$ whereas for $\kappa=0.12$ tunneling is no longer observed, on our largest, 16^3, lattice. The double-peak structure of $|\Omega|$ for $\kappa=0.10$ is seen in Fig. 5 where it is fitted to the sum of two Gaussian distributions in the complex plane, one centered at the origin (confined phase) and one centered at a fitted location along the real axis (deconfined phase). The second peak seems to approach the first as the lattice size increases, which would indicate a second- rather than a first-order transition. A double-peak structure was also observed for $\kappa=0.05$ but the distance between the peaks remains the same as the lattice size increased. For $\kappa=0.12$ the double peak was no longer visible.

In Fig. 6 we show the deconfinement ratio ρ as a function of β, using reweighting [24], for $\kappa=0.05$, 0.10, and 0.12 as well as for the quenched case ($\kappa=0$). The latter is included as a check of our methodology and statistical accuracy. Our quenched data have similar statistics to our full QCD data. The intersection of the deconfinement ratio curves $\rho(\beta)$ for various lattice sizes occurs very near the known value of β_c [3], shown by an asterisk, and around a value 3/4 for the deconfinement ratio. The largest lattice (24^3) results, actually obtained by reweighting data from our effective model (see Sec. V), help determine the critical point more accurately, but are not necessary to ascertain the transition itself. A qualitative change is seen to occur around $\kappa=0.10$; namely, the curves for various lattice sizes stop intersecting. In fact for $\kappa=0.14$, which is not represented, the deconfinement ratio always stays very near 1.

A similar qualitative change is visible in Fig. 7, which shows the susceptibility χ_L divided by the volume, again reweighted as a function of β. For $\kappa=0$ and 0.05, the peak of χ_L/V is almost independent of V. In other words, χ_L diverges like V, as befits a first-order transition. For all the higher κ's, χ_L/V decreases as the volume grows, indicating that the first-order transition has disappeared or that the asymptotic behavior has not yet set in.

We use the peak of the Polyakov loop susceptibility χ_L to determine the pseudocritical coupling $\beta_c(\kappa)$. The dotted lines in Fig. 7 delimitate a band where χ_L is near its peak

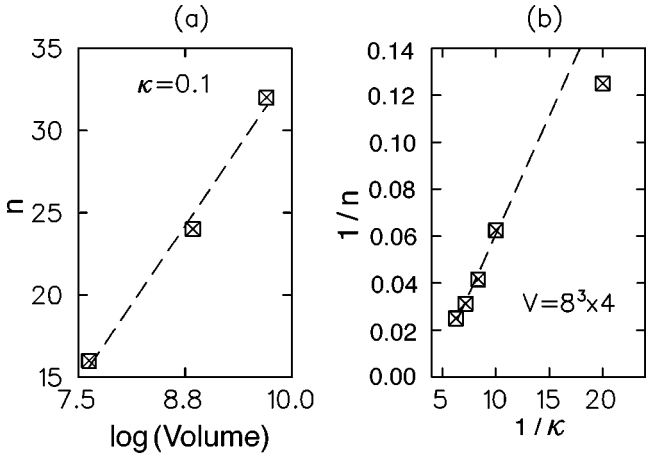

FIG. 3. (a) The number of bosonic fields, n, is plotted vs the logarithm of the volume for $\kappa=0.1$. (b) $1/n$ vs $1/\kappa$ for the $8^3\times4$ lattice.

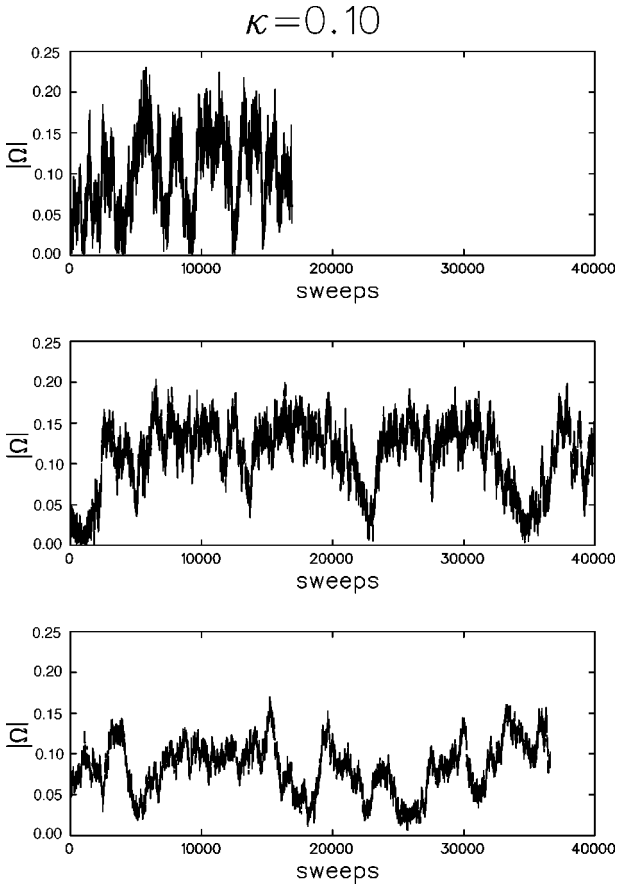

FIG. 4. Monte Carlo history of the Polyakov loop for $\kappa=0.10$ on lattices $8^3\times4$, $\beta=5.670$ (upper), $12^3\times4$, $\beta=5.670$ (middle), and $16^3\times4$, $\beta=5.660$ (lower).

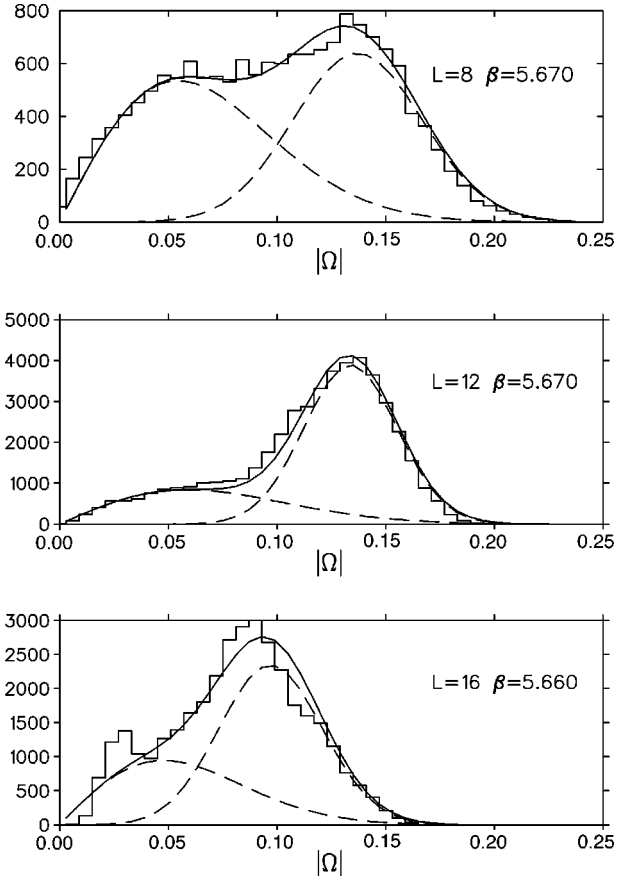

FIG. 5. Double-peak structure of $|\Omega|$ for $\kappa=0.10$ fitted to a sum of two Gaussians, centered at the origin and at an adjustable position on the real axis.

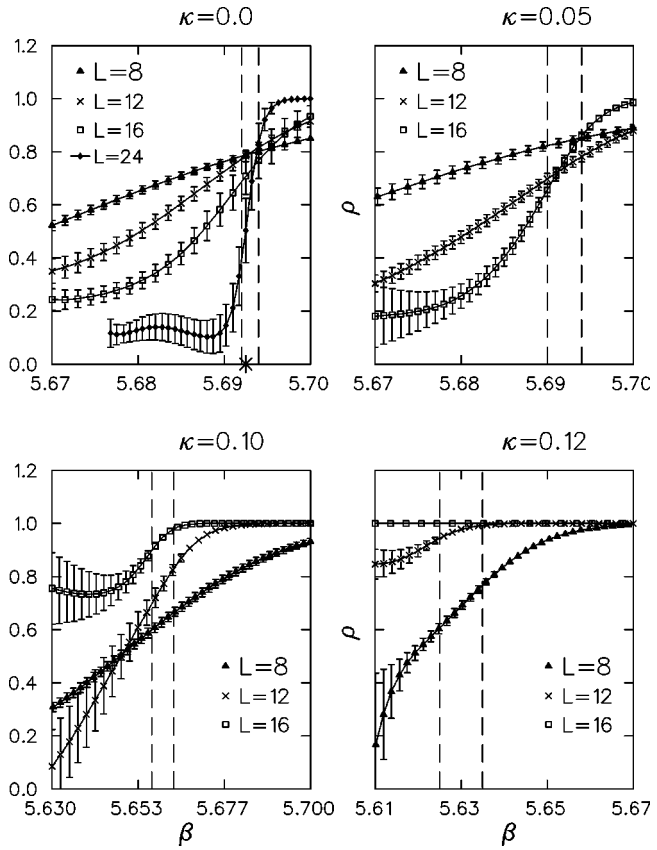

FIG. 6. Deconfinement ratio for $\kappa=0.05$, $\kappa=0.10$, and $\kappa=0.12$ for three lattice sizes. The dashed lines give the error band for the critical β value as determined from the maximum of the susceptibility (see Fig. 7). The asterisk denotes the quenched result for β_c from Ref. [3].

value on our largest volume. These bands, also shown in Fig. 6, display the nice agreement between this criterion and the crossing of the deconfinement ratio lines when that takes place. We have also looked at the average of the real part of the Polyakov loop Ω after projection to the closest $Z(3)$ axis, and found that the position where data from different lattices cross is again within the same error band. Our values for $\beta_c(\kappa)$ are collected in Table II and plotted in Fig. 8. Comparing them with available β_c values for $N_f=2$ [25], also included in Table II, we see that the effect of one dynamical quark on the value of β_c is to shift it from the quenched result of $\beta_c=5.6923(4)$ by about half the amount of the shift produced by two degenerate quarks for the same κ value. Not surprisingly, when the dynamical quarks are heavy, their ordering effect grows linearly with the number of flavors. One could therefore use our $N_f=1$ data to complete the blank $N_f=2$ entries in Table II.

The volume dependence of the peak value of χ_L is more clearly displayed in Fig. 9a. The lines shown are best fits to the form V^α. As discussed in Sec. III, values $\alpha=1$, $0<\alpha<1$ and 0 characterize a first-order transition, second-order transition, or crossover, respectively, up to finite-size corrections. For $\kappa=0.05$ the best fit yields $\alpha=0.96(4)$, to be compared to the pure gauge value $\alpha=1.02(4)$ for which the data are plotted in Fig. 9b. The transition is first order. For $\kappa=0.14$, on the other hand, we find $\alpha=0$, a clear signal of crossover behavior. For $\kappa=0.10$ and $\kappa=0.12$ the situation is less clear. The small value of $\alpha=0.22(3)$ at $\kappa=0.12$ favors the crossover region. For $\kappa=0.10$, $\alpha=0.56(3)$, and we must be quite near the second-order end point.

We summarize our findings.

For $\kappa=0.05$ all our observables [tunneling, intersecting deconfinement ratios $\rho(\beta)$, linear dependence of the susceptibility peak on V] behave quite similarly to the quenched case and consistently point to a first-order transition.

For $\kappa=0.12$ and 0.14, all our observables (no tunneling, no crossing of the deconfinement ratios, growth of the susceptibility peak slow or nonexistent) point to a crossover.

For $\kappa=0.10$, the situation is less clear. On the largest lattice, we do not see the signals of a phase transition: tunneling is suppressed as compared to $\kappa=0.05$, the peak in the Polyakov loop distribution moves towards the origin, the deconfinement ratio does not intersect the smaller volume curves, and the peak of the Polyakov loop susceptibility is not much larger than the peak value for the next smaller volume. Based on this largest volume, we consider $\kappa=0.10$ as being close to the end point, but rather on the crossover side.

A more precise statement would require simulations on larger lattices. Larger volumes together with a more refined finite size scaling (FSS) ansatz would lead to a precise de-

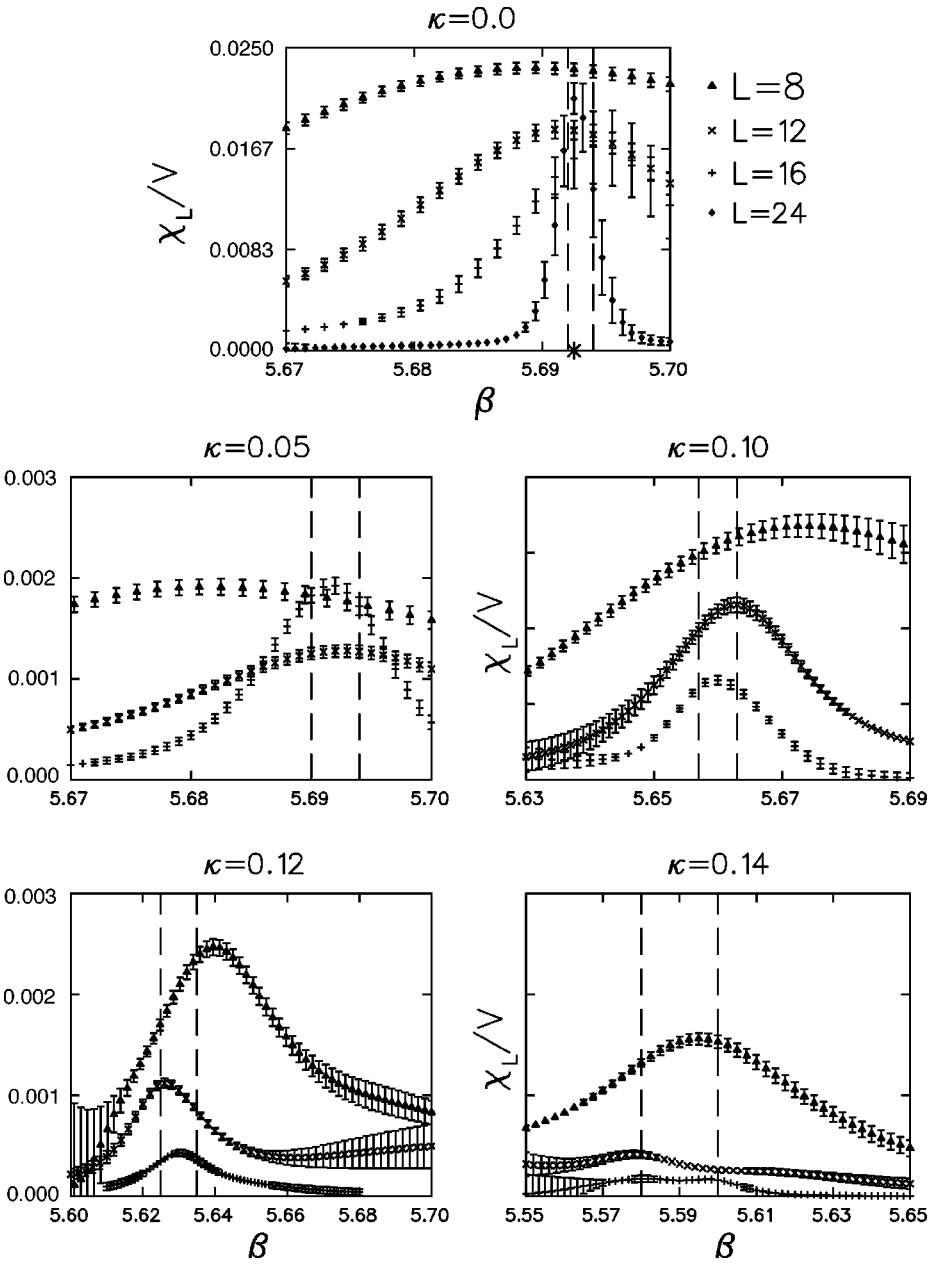

FIG. 7. The susceptibility per unit volume for the quenched theory ($\kappa=0$) and for $\kappa=0.05$, $\kappa=0.10$, $\kappa=0.12$, and $\kappa=0.14$. The asterisk marks β_c [3] for the quenched theory.

termination of the end point. We carry out this approach in the context of the effective model discussed in detail in the next section.

V. EFFECTIVE MODEL

It is clear from the above results that locating the end point (β_{ep},κ_{ep}) accurately requires very large lattice sizes, beyond our computer capabilities. We thus adopt a different approach: We consider an effective model, in the same universality class as full QCD but cheaper to simulate. By simulating larger systems, we locate the end point in the coupling plane of this model. Then we map this end point back onto full QCD.

TABLE II. The pseudocritical β value is given for the four κ values studied. The two-flavor results are from Ref. [25] and are given for comparison. The quenched result from [3] is $\beta_c=5.6923(4)$.

	κ	0.05	0.10	0.12	0.14
$N_f=1$	β_c	5.692(2)	5.660(3)	5.630(5)	5.59(1)
$N_f=2$	β_c			5.58(2)	5.46(2)

The simplest prototype of our universality class is the three-dimensional three-state Potts model in an external field h:

$$S=-\sum_{\langle nl\rangle}\beta\,\mathrm{Re}\,z_n^*z_l-h\sum_n\mathrm{Re}\,z_n,\quad h>0, \tag{16}$$

with z_n an element of $Z(3)$. Dimensional reduction at high temperature reduces QCD to this model. Quenched QCD maps onto the $Z(3)$-symmetric $h=0$ version, which undergoes a first-order transition at $\beta_c\approx 0.55053$ [26]. Full QCD

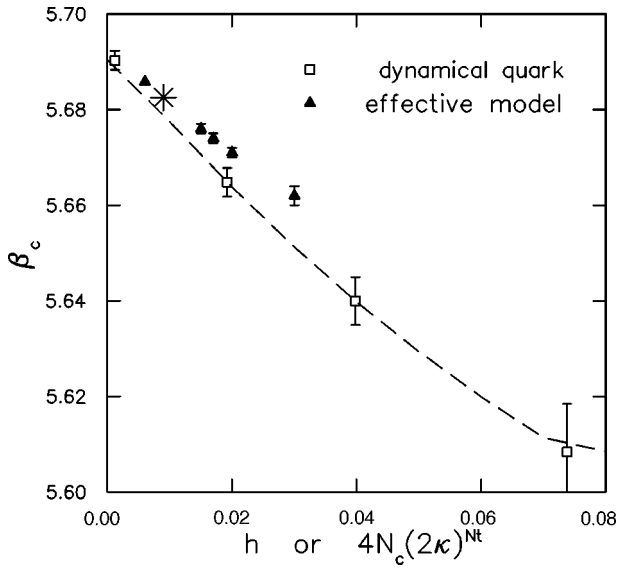

FIG. 8. The pseudocritical deconfinement coupling β_c as a function of κ^{N_t} (open squares) found from the analysis of the QCD data with one dynamical quark species (here $N_t=4$). The dashed line is to guide the eye. The results for the same quantity obtained for our effective model (Sec. V) are also plotted as a function of the field strength h. The asterisk shows the second-order end point. The QCD data are shifted upwards by $16N_c\kappa^4$ to take into account an effective change in β coming from expanding the fermionic determinant up to order κ^4.

reduces to the $h>0$ version, where the strength of the $Z(3)$-breaking field h grows with the inverse quark mass. That model has been studied by DeGrand and DeTar [15]. They found a first-order transition line in the plane (β,h), ending at (β_{ep},h_{ep}) (see Fig. 1). The second-order end-point critical field h_{ep} was evaluated in the mean-field approximation, yielding the small value $\frac{2}{3}\log 2-\frac{4}{9}\sim 0.018$, and by Monte Carlo simulations where the estimate $10^{-3}<h_{ep}<10^{-2}$ was obtained. Unfortunately the mapping from h_{ep} back to a quark mass is qualitative rather than quantitative. This is why we have to turn to a more complicated, four-dimensional model.

The starting point is the fermionic determinant which can be expanded into loops, yielding

$$\det(\mathbf{1}-\kappa M)=\exp\left(-\sum_l \frac{\kappa^l}{l}\mathrm{Tr}(M^l)\right). \tag{17}$$

This expansion will converge quickly for the range of κ's under consideration. The loops which are relevant for the breaking of the $Z(3)$ symmetry are the ones that wind around the time direction. Among them the shortest and most important is the Polyakov loop, Eq. (12), which carries a coefficient $(2/N_t)(2\kappa)^{N_t}$ on a lattice of time dimension N_t. Our effective model tries to incorporate higher-order effects with an effective $Z(3)$-breaking field h and an action

$$S_{\mathrm{eff}}=S_g[U]-h(\kappa)\sum_{\mathbf{x}}\mathrm{Re}\,\mathrm{Tr}\,L(\mathbf{x}). \tag{18}$$

Besides the leading hopping parameter expansion above, which should be accurate at small κ, the mapping $h(\kappa)$ can be obtained in other ways. One way is to resum all spatial hoppings within the free approximation, so that

$$h(\kappa)=N_t\int_{-\pi}^{\pi}\frac{d^3q}{(2\pi)^3}\mathrm{Tr}[(1+\gamma_0)\kappa G(q)]^{N_t}, \tag{19}$$

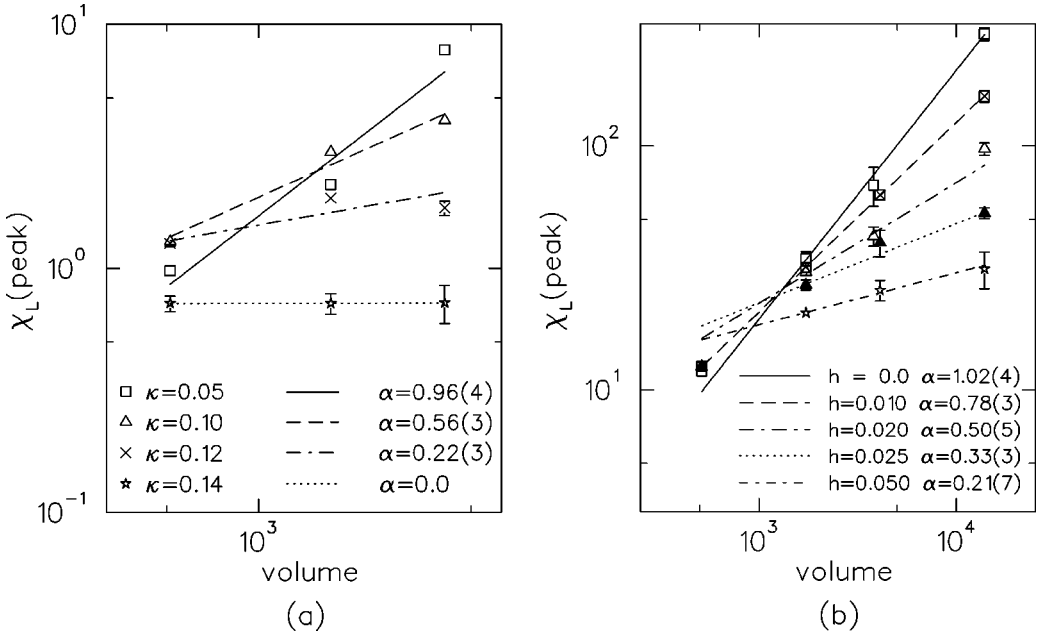

FIG. 9. (a) The volume dependence of the peak of the susceptibility for $\kappa=0.05$, $\kappa=0.10$, $\kappa=0.12$, and $\kappa=0.14$. (b) The volume dependence of the peak of the susceptibility in our effective model (Sec. V) for $h=0.01$, $h=0.02$, $h=0.025$ and $h=0.05$. A couple of points are slightly shifted in volume for clarity.

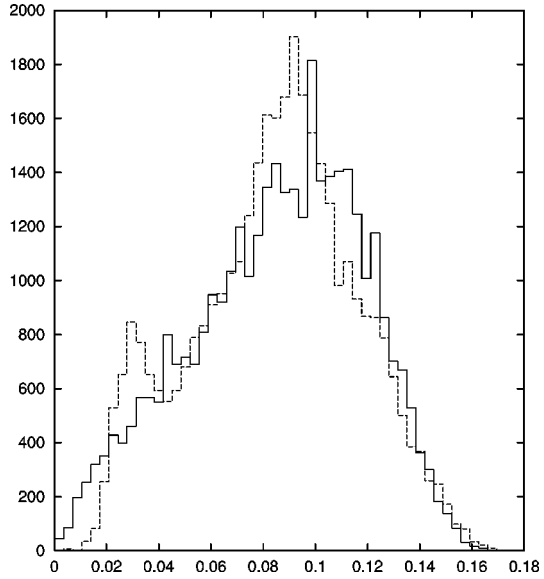

FIG. 10. Best fit of $|\Omega|$ from full QCD for $\kappa=0.1$ (dashed line) to the data obtained from the effective model using reweighting (solid line for $h=0.026$).

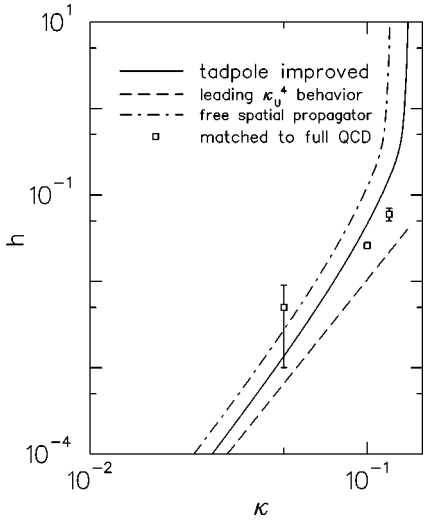

FIG. 11. The strength of the $Z(3)$-breaking term versus κ.

where $G(q)^{-1}$ is the free spatial quark propagator. This mapping incorporates the divergence of h when $\kappa\to\kappa_c$, with $\kappa_c=1/8$. This result can be further refined by considering tadpole improvement, such that κ in Eq. (19) is substituted by $\kappa\langle plaq\rangle^{1/4}$. Finally, a nonperturbative approach consists in finding the best match $h(\kappa)$ between the distribution of the magnitude of the Polyakov loop Ω [Eq. (13)] in full QCD and that in the effective model. The quality of such a matching is illustrated in Fig. 10. At lower κ or h, this nonperturbative matching becomes more sensitive to statistical fluctuations in the exploration of $Z(3)$ sectors, which can mimic a symmetry-breaking term. In that regime the other, analytical methods work better. Our nonperturbative matching results of the whole Ω distribution are listed in Table III. (Matching the first two moments of the distribution gave consistent results.) Figure 11 compares the various mappings $h(\kappa)$ considered here.

Now, equipped with a reasonably accurate correspondence between h and κ, we can look for the critical line (β,h) and its end point in our effective model. We simulate lattices of spatial size 8^3, 12^3, 16^3, and 24^3 with the temporal direction fixed at $N_t=4$ as in the case of the full QCD simulations. We obtain data at various values of $h=0.01$, 0.02, 0.025, and $h=0.05$ with typically 10 000–20 000 thermalized configurations.

First, we perform the same analysis, using the same observables as in Sec. IV for full QCD. At each value of h, we identify the pseudocritical coupling $\beta_c(h)$ and obtain the points included in Fig. 8, which for small κ follow closely the corresponding curve obtained in full QCD. In Fig. 9b we show the dependence of the peak of the Polyakov loop susceptibility χ_L on the spatial volume for various values of $h(\kappa)$. The behavior is again very similar to that of full QCD, indicating a weakening of the first-order phase transition as h increases and probably a crossover behavior for $h\geqslant 0.03$.

TABLE III. Nonperturbative determination of h by fitting to the QCD data. The value of h listed here gave the best fit to the QCD data of the $|\Omega|$ distribution.

κ	0.05	0.10	0.12
h	0.005(4)	0.026(2)	0.06(1)

Now we would like to determine as precisely as possible the end point (β_{ep},h_{ep}) and check the scaling behavior in its vicinity. In Ref. [27] the same issues were addressed in the context of the electroweak theory, and a reliable numerical procedure was presented which yielded impressively accurate answers. The procedure we follow is very similar, although not quite identical. From our Monte Carlo data we obtain the joint probability distribution of the plaquette and the real part of the Polyakov loop (shown in Fig. 12). The principal axes of this distribution, which diagonalize the correlation matrix of the two observables, are identified as the magnetizationlike variable M and the energylike variable E. (The rotated distribution displayed in Fig. 13 shows the double-peak distribution in the M-like direction.) After subtracting the averages from the new variables M and E such that $\langle M\rangle=\langle E\rangle=0$, rescaling them such that $\langle M^2\rangle=\langle E^2\rangle=1$, and reweighting in β and h, we obtain the probability density $P(M,E)$ shown in Fig. 14 at the end point. We clearly see that the marginal distribution $P(E)$ will show a single peak, while $P(M)$ will have a double peak. In an infinite volume the distribution $P(M)$ would be symmetric. Comparing the $P(M,E)$ distribution of Fig. 14 with the 3 dimensional (3d) results of Fig. 3 of Ref. [27] for the Ising model and the $O(2)$ and $O(4)$ models, our result is in closest agreement with the $P(M,E)$ distribution of the Ising model.

To determine the end point we need to perform a finite-size scaling analysis. For each lattice size, we reweight in β and h until we minimize the asymmetry of the M distribution, by requiring the vanishing of the third cumulant:

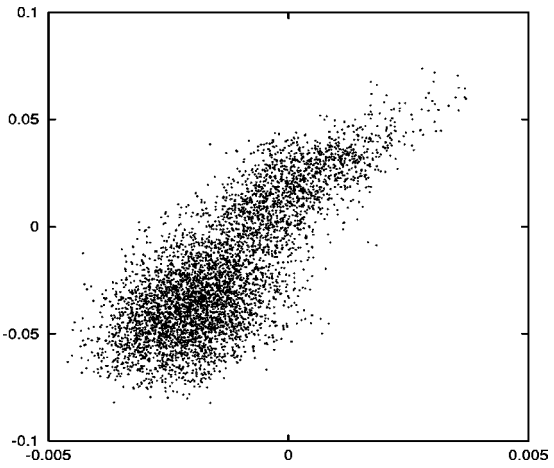

FIG. 12. $(S_{\rm eff}-\langle S_{\rm eff}\rangle)$ vs $(S_g-\langle S_g\rangle)$ for 5000 configurations on 24^3 at $h=0.01$, $\beta=5.680$.

$$\frac{\langle M^3\rangle}{\langle M^2\rangle^{3/2}}=0. \tag{20}$$

This determines a line in the plane (β,h), which must go through the infinite-volume critical point (β_{ep},h_{ep}), up to statistical errors. The intersection of these lines obtained for various lattice sizes therefore determines the critical point (β_{ep},h_{ep}). Parametrizing these lines by the value of h, we show in Fig. 15 the variation of the fourth magnetic cumulant,

$$\frac{\langle M^4\rangle}{\langle M^2\rangle^2}, \tag{21}$$

along these lines, for the three largest lattices considered for $N_t=4$ as well as for three lattices for $N_t=2$. The simulation of the effective model at $N_t=2$ using spatial sizes 8, 12, and

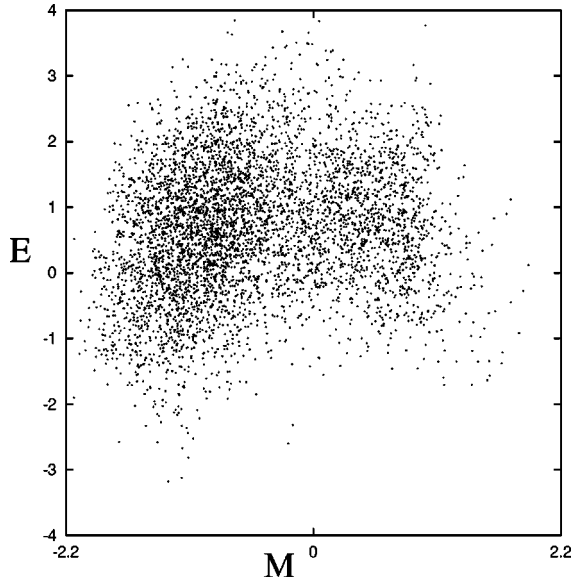

FIG. 13. $(S_{\rm eff}-\langle S_{\rm eff}\rangle)$ vs $(S_g-\langle S_g\rangle)$ for 5000 configurations on 24^3 at $h=0.01$, $\beta=5.680$ after a rotation.

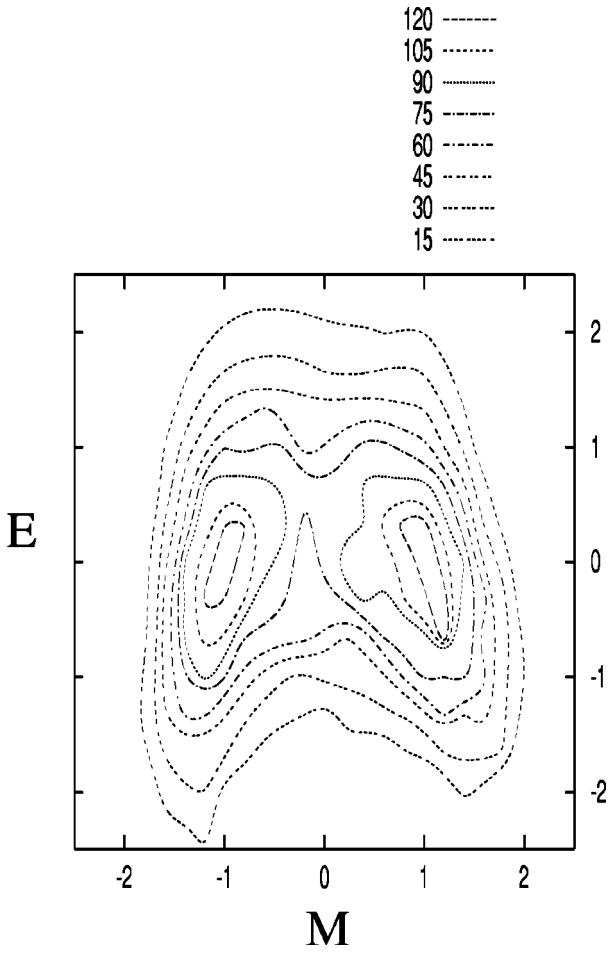

FIG. 14. Normalized probability distribution at the critical point $h_{ep}=0.009$ for 24^3.

16 can be used as a check of our procedure in a situation where significant deviations from scaling are not expected. The three lines for $N_t=2$ cross at a point which gives the critical end point. The fact that the three lines meet at a point (within statistical errors) indicates stability against deviations from scaling. Note that we made no assumption about the universality class in our determination of the critical point. Because of its generality and because of its relative statistical robustness in our case, we favor the method we just described to find the end point over the method used in Ref. [27], which fixes the fourth cumulant, Eq. (21), to its Ising value. The value of $\langle(\Delta M)^4\rangle/\langle(\Delta M)^2\rangle^2$ at the critical end point can now be used to check the universality class of the effective model and thus the universality class of QCD. From Fig. 15(a) at $h_{ep}=0.06$ we find $\langle(\Delta M)^4\rangle/\langle(\Delta M)^2\rangle^2 \sim 1.67(5)$ in good agreement with the corresponding value of 1.604(1) for the Ising model.[2] The value of β_{ep} determined from the crossing of the lines parametrized with the value of β is $\beta_{ep}=5.047(1)$. For $N_t=4$ the lines for our

[2]For the $O(2)$ and $O(4)$ models $\langle(\Delta M)^4\rangle/\langle(\Delta M)^2\rangle^2=1.233(6)$ [28] and 1.092(3) [29], respectively, i.e., clearly lower than our value of 1.67(5).

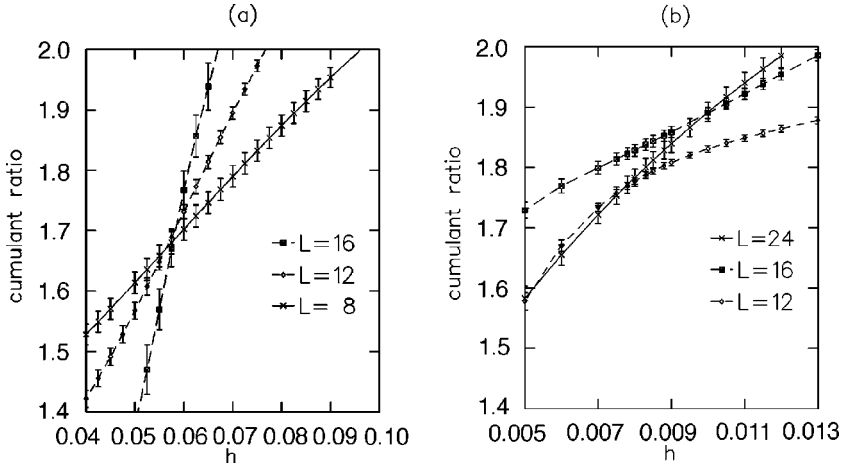

FIG. 15. The fourth magnetic cumulant versus the field strength h: (a) for $N_t=2$, (b) for $N_t=4$. The point of intersection of the lines determines the critical point h_{ep}.

three largest volumes converge at $h\sim 0.009$. Scaling violations are still seen for the lattice with spatial extent $L=12$. Thus here the end point is determined less accurately as compared to the $N_t=2$ case, although we have increased our statistics fivefold using ~ 100000 configurations for the two smaller lattices and ~ 50000 for the largest lattice. Since the point of intersection for the two largest lattices is within statistical errors consistent with $h=0.009$, we take $h_{ep}\sim 0.009(1)$ as the best determination of the critical point from these data. Having determined the critical point we can look at critical exponents. The magnetic susceptibility at h_{ep} should scale like [27]

$$\chi_M = V\langle(\Delta M)^2\rangle \propto L^{-3+\gamma/\nu}. \tag{22}$$

We plot the χ_M distributions in Fig. 16 for our three lattices after scaling with $L^{-0.8}$. They are seen to nicely fall on top of each other. This scaling thus yields a rough estimate of the exponent $\gamma/\nu\sim 2.2$ to be compared with a value of 1.96 for the Ising, $O(2)$, and $O(4)$ models. To determine exponents such as α/ν which can pin down the Ising model universality class we need to consider the scaling behavior of the E-like variable, which is smaller than the M-like variable by at least two orders of magnitude. Scaling based on the E-like variable was found to be unstable within the statistical precision of our present simulation.

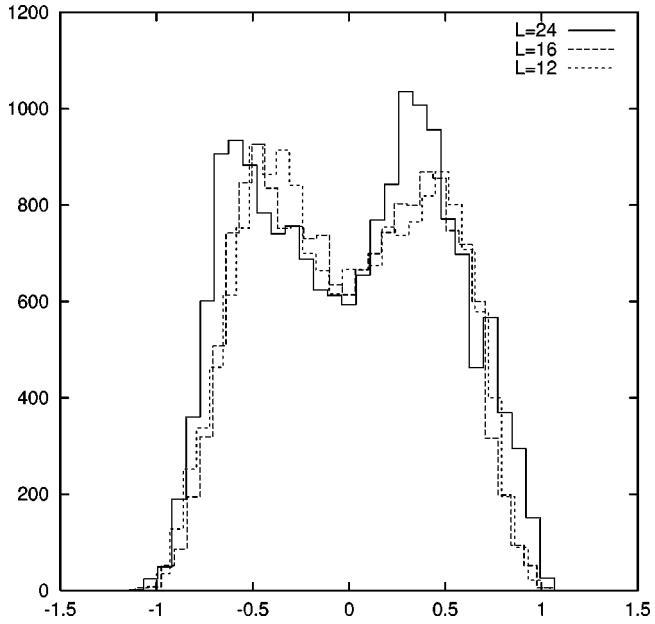

FIG. 16. Scaling of the M-like distribution at the critical point h_{ep} and β_{ep} for the three largest lattices. We have applied a scaling factor of $L^{-0.8}$ to all the data.

Finally, we comment on the Polyakov distribution displayed in Fig. 14. It is clear from this figure that even at the end point $h_{ep}=0.009$, the Polyakov loop distribution still shows a marked double-peak structure. In Ref. [30] where the same effective model was studied, the criterion used to identify the end point was to look for the value of h where the double-peak structure of the real part of the Polyakov loop was no longer visible. This criterion thus led to a much bigger value ~ 0.08 for the critical field strength than we are finding here.

VI. DISCUSSION

From the previous section we conclude that the end point of the first-order transition occurs at $h(\kappa)\sim 0.009$ which maps to $\kappa\sim 0.08$. The qualitative picture expected for $(2+1)$ flavors in the continuum is that there is a finite region in the mass plane $(m_{u,d}, m_s)$ of the two degenerate flavors versus the third near the quenched limit where the deconfinement phase transition is first order. Our $N_f=1$ result corresponds to the infinite-mass limit for $m_{u,d}$. In this limit, which up to now received little attention, we find that the first-order pure gauge phase transition persists up to $\kappa\sim 0.08$. Since we expect dynamical quark effects to be twice as strong for two flavors (see Table II), we can estimate the boundary of the first-order region as

$$2h_{eff}(k_{u,d}) + h_{eff}(k_s) \approx 0.009, \tag{23}$$

with $h_{eff}(\kappa)$ as per Fig. 11.

It is of course of crucial importance to establish the scaling behavior of our results and to express the end-point parameter as a quark mass, not a hopping parameter. One might wonder if the rather small value of κ_{ep} we found may not be an artifact of the relatively coarse lattice discretization and if one would recover $\kappa_{ep}=0$ in the continuum limit. This would mean that the deconfinement transition disappears as soon as dynamical quarks of any mass are allowed. Such a scenario goes against the robustness of a first-order phase transition. The first-order deconfinement transition must be robust against small variations of the parameters, before ending at a second-order point. We made this argument in the Introduction to justify the expected phase diagram, Fig. 1, in our discrete theory. The same argument applies to the continuum QCD theory. Therefore, we expect the deconfinement transition to end at a finite quark mass m_q. Determining this mass would require a full-blown scaling study of one-flavor QCD, which is beyond the scope of this paper. However, we have considered what happens to our effective model as the lattice spacing a changes. We have simulated our effective model for $N_t=2$ and found $h_{ep} \approx 0.06$, with scaling exponents consistent with those at $N_t=4$. Changing $N_t=4$ to $N_t=2$ amounts to doubling the lattice spacing a. Therefore, the variation of the end-point value h_{ep} indicates a scaling behavior

$$h_{ep}(2a)/h_{ep}(a) \approx 0.06/0.009 \propto a^{2.7}. \tag{24}$$

This strongly supports the existence of a continuum limit for the effective model, Eq. (18), with the action

$$S_{eff}=S[A]-\tilde{h}\int d^3x L(\mathbf{x}), \tag{25}$$

where $h=\tilde{h}a^3$ in the discretized theory, having a critical end point at some positive $\tilde{h}_{ep}$.

If one believes in the physical nature of the critical coupling $\tilde{h}_{ep}$, then the corresponding quark mass cannot be infinite. For instance, the leading hopping parameter expansion, Eq. (17), at constant physical temperature $T=(N_t a)^{-1}$ gives

$$h(\kappa) \sim 4N_c(2\kappa)^{(aT)^{-1}}. \tag{26}$$

If $h(\kappa)=\tilde{h}_{ep}a^3$, then this relation is not consistent with $\lim_{a\to 0}\kappa=0$. One is again led to expect persistence of the first-order transition, for some range of quark mass, in the continuum one-flavor QCD theory.

We can get an estimate of the critical quark mass in physical units by using the naive prescription $m_q a=\frac{1}{2}(1/\kappa - 1/\kappa_c)$. Using the quenched data of Ref. [31] for the pion mass we find $\kappa_c=0.1694(2)$, at $\beta=5.7$ in the zero-flavor theory. On the other hand, the SESAM Collaboration finds $\kappa_c=0.1585(1)$ [32] at $\beta=5.6$ in the two-flavor theory. Going to our value of $\beta_{ep}=5.683(3)$ will decrease the critical value from SESAM slightly. If we neglect this change and take the average between the zero- and two-flavor cases, we end up with $\kappa_c \approx 0.164$. Taking the end-point value $\kappa_{ep} \sim 0.08$ we find a quark mass $m_q a=3.2$ in units of the lattice spacing a. This mass is in fact of the same order as that of the doubler modes, which leads to an overestimation of the mass at the end point. Since $m_q a>1$, finite-a corrections are expected to be rather large. At the tree level the corrected mass is given by

$$m_q a \sim \frac{m_q a}{\sqrt{1+m_q a}}, \tag{27}$$

which reduces our estimate by about a factor of 2 to $m_q a \sim 1.56$. To convert this to physical units we use $(4a)^{-1} \sim 220$ MeV from the deconfinement temperature. This gives $m_q \sim 1.4$ GeV for the end point.

A critical quark mass of the order of 1 GeV is in line with phenomenological expectations. The pure gauge deconfinement transition is fairly weak, with a critical correlation length $\xi_c \sim (7-10)a$ at $\beta=6$ [25], i.e. ~ 11 GeV^{-1} or $\mathcal{O}(5\sigma^{-1/2})$. This is the minimum system size necessary to observe the first-order nature of the deconfinement transition. Dynamical quarks introduce a new length scale r_c, namely, the distance where the string breaks, $r_c \sim \mathcal{O}(2m_q/\sigma)$. Confinement can only be observed up to this distance. For very heavy quarks, $r_c > \xi_c$: string breaking occurs for a large separation, larger than the critical correlation length. The passage from confinement to deconfinement will allow ''liberated'' quarks to appear even if their separation is less than r_c. This qualitative change signals a phase transition. As the quark mass is lowered, the string-breaking scale r_c decreases. When $r_c \sim \xi_c$, the passage from confinement to deconfinement does not liberate quarks that were not already liberated by string breaking. There is no qualitative change from one regime to the other, and one cannot really tell if the system is confined or deconfined: the phase transition has disappeared and been replaced by a crossover. This occurs for

$$m_q \sim \mathcal{O}(5\sqrt{\sigma}/2), \quad \text{i.e.,} \quad m_q \sim \mathcal{O}(1) \text{ GeV}. \tag{28}$$

VII. SUMMARY AND CONCLUSIONS

The multiboson method can be used to simulate an odd number of flavors as well as an even number. In this work we have shown that the multibosonic algorithm is well suited for the study of one-flavor QCD for moderately heavy Wilson quarks. Using this algorithm we were able to carry out a detailed finite size scaling analysis to determine the pseudocritical $\beta(\kappa)$ line for κ values up to $\kappa=0.14$. We demonstrated that the first-order phase transition seen in the quenched theory persists when one includes dynamical quarks. Using FSS we showed that the deconfinement phase transition gets weaker as the dynamical quark mass increases and then turns into a crossover. In general we find that the dynamical quark effects on the phase transition are approximately half those for two flavors. Using lattices of sizes 8^3, 12^3, and $16^3 \times 4$ within full QCD, we found an end point around $\kappa=0.1$. A more accurate determination would require simulation of larger spatial volumes. In order to carry out a more refined FSS analysis with larger lattices we considered an effective model in the same universality class as full

QCD. In this effective model the effects of the fermionic determinant were simulated by an effective $Z(3)$-breaking field coupled to the Polyakov loop. We studied the phase transition as a function of this field strength h on lattices with spatial volumes 8^3, 12^3, 16^3, and 24^3 and found a first-order transition that gets weaker as the field strength increases, exactly like in QCD as κ increases. Performing a FSS analysis using the joint probability distribution of the plaquette and the real part of the Polyakov loop we were able to determine, without any assumptions about the universality class of the model, the end point of the first-order transition line. Matching of the Polyakov loop histograms or its first two moments in the effective model to those in full QCD enabled us to determine nonperturbatively the correspondence between h and κ. In this way we obtained the value of $\kappa_{ep} \sim 0.08$ for the end point of the QCD first-order transition line. Futhermore, the FSS analysis of the effective model at the critical point yielded results consistent with our effective model being in the same universality class as the Ising model. Although a FSS analysis was not possible for QCD, this finding is important in suggesting that the universality class of one-flavor QCD and the Ising model may be the same.

We have also studied our effective model on a coarser lattice at $N_t = 2$, and have found good scaling behavior of the end point field strength, with similar Ising-like exponents at the end point. This scaling test strongly supports the existence of a critical end point at a nonvanishing positive field strength in the continuum limit of our effective model. In turn, this indicates a nonvanishing quark mass for the end point of the deconfinement transition line $T_c(m_q)$ in continuum one-flavor QCD. Our findings are in agreement with the idea that a first-order transition is robust against small variations of the parameters, before ending at a second-order point. Converting the value of $\kappa_{ep} = 0.08$ to physical units can only be done approximately, using quenched and two-flavor determinations of κ_c at similar β values. After correcting for finite lattice spacing errors to the tree level we obtain an estimate of the quark mass at the end point of $m_q \sim 1.4$ GeV, consistent with phenomenological expectations. A simulation of one-flavor QCD closer to the continuum limit would allow tighter control over discretization errors, but is beyond our computer resources.

ACKNOWLEDGMENTS

We thank SIC of the EPFL in Lausanne, ZIB in Berlin, and the Minnesota Supercomputing Institute for providing the necessary computer time. P.dF. would like to thank M. Ogilvie, K. Rummukainen, A. J. van der Sijs, J. Zinn-Justin, and C. A. B. Svetitsky for discussions.

[1] A. M. Polyakov, Phys. Lett. **72B**, 477 (1977).
[2] L. Susskind, Phys. Rev. D **20**, 2610 (1978).
[3] M. Fukugita, M. Okawa, and A. Ukawa, Nucl. Phys. **B337**, 181 (1990).
[4] Y. Iwasaki *et al.*, Phys. Rev. D **46**, 4657 (1992).
[5] R. G. Edwards, U. M. Heller, and T. R. Klassen, Nucl. Phys. **B517**, 377 (1998).
[6] G. Boyd, J. Engels, F. Karsch, E. Laermann, C. Legeland, M. Lutgemeier, and B. Petersson, Phys. Rev. Lett. **75**, 4169 (1995); Nucl. Phys. **B469**, 419 (1996).
[7] T. DeGrand *et al.*, Nucl. Phys. **B454**, 615 (1995).
[8] B. Beinlich, F. Karsch, E. Laermann, and A. Peikert, Eur. Phys. J. C **6**, 133 (1999).
[9] MILC Collaboration, C. Bernard *et al.*, Phys. Rev. D **61**, 5584 (1997).
[10] E. Laermann, Nucl. Phys. B (Proc. Suppl.) **63**, 114 (1998); K. Kanaya, Prog. Theor. Phys. Suppl. **131**, 73 (1998).
[11] Y. Iwasaki, K. Kanaya, S. Kaya, S. Sakai, and T. Yoshié, Prog. Theor. Phys. Suppl. **131**, 415 (1998).
[12] M. Fukugita, S. Ohta, and A. Ukawa, Phys. Rev. Lett. **60**, 178 (1988); M. Fukugita and A. Ukawa, Phys. Rev. D **38**, 1971 (1988).
[13] R. D. Pisarski and F. Wilczek, Phys. Rev. D **29**, 338 (1984).
[14] Sh. Chandrasekharan and N. Christ, Nucl. Phys. B (Proc. Suppl.) **47**, 527 (1996).
[15] T. A. DeGrand and C. E. DeTar, Nucl. Phys. **B225**, 590 (1983).
[16] C. Alexandrou, A. Borici, Ph. de Forcrand, A. Galli, F. Jegerlehner, and T. Takaishi, Nucl. Phys. B (Proc. Suppl.) **53**, 435 (1997); **63**, 406 (1998).
[17] M. Lüscher, Nucl. Phys. **B418**, 637 (1994).
[18] A. Borrelli, Ph. de Forcrand, and A. Galli, Nucl. Phys. **B477**, 809 (1996).
[19] A. Boriçi and Ph. de Forcrand, Nucl. Phys. **B454**, 645 (1995).
[20] Ph. de Forcrand, in ''Lattice '98,'' Boulder, Colorado 1998, hep-lat/9809145.
[21] B. Svetitsky and L. G. Yaffe, Nucl. Phys. **B210**, 423 (1982); B. Svetitsky, Phys. Rep. **132**, 1 (1986).
[22] M. S .S. Challa, D. P. Landau, and K. Binder, Phys. Rev. B **34**, 1841 (1986); K. Binder and D. P. Landau, *ibid.* **30**, 1477 (1984); M. E. Fisher and A. N. Berker, *ibid.* **26**, 2507 (1982).
[23] Ph. de Forcrand, Nucl. Phys. B (Proc. Suppl.) **47**, 228 (1996).
[24] A. M. Ferrenberg and R. H. Swendsen, Phys. Rev. Lett. **63**, 1195 (1989).
[25] S. Aoki, A. Ukawa, and T. Umemura, Phys. Rev. Lett. **76**, 873 (1996).
[26] W. Janke and R. Villanova, Nucl. Phys. **B489**, 679 (1997).
[27] K. Rummukainen, M. Tsypin, K. Kajantie, M. Laine, and M. Shaposhnikov, Nucl. Phys. **B532**, 283 (1998).
[28] A. P. Gottlob and M. Hasenblusch, Report No. CERN-TH.6885/93.
[29] K. Kanaya and S. Kaya, Phys. Rev. D **51**, 2404 (1995).
[30] P. N. Meisinger and M. C. Ogilvie, Phys. Rev. D **52**, 3024 (1995).
[31] F. Butler, H. Chen, J. Sexton, A. Vaccarino, and D. Weingarten, Nucl. Phys. **B430**, 179 (1994).
[32] SESAM Collaboration, N. Eicker *et al.*, Phys. Lett. B **407**, 290 (1997).